Molecular Crystals and Liquid Crystals

Publication details, including instructions for authors and subscription information:
http://www.tandfonline.com/loi/gmcl20

Influence of Alkyl Chain Length on the Solid-State Packing and Fluorescence of 1,4,5,8-Tetra(alkyl)anthracenes

Chitoshi Kitamura [a], Yasushi Abe [a], Nobuhiro Kawatsuki [a], Akio Yoneda [a], Kohei Asada [b], Takashi Kobayashi [b] & Hiroyoshi Naito [b]

[a] Department of Materials Science and Chemistry, Graduate School of Engineering, University of Hyogo, Himeji, Hyogo, Japan

[b] Department of Physics and Electronics, Graduate School of Engineering, Osaka Prefecture University, Sakai, Osaka, Japan

Version of record first published: 22 Sep 2010

To cite this article: Chitoshi Kitamura, Yasushi Abe, Nobuhiro Kawatsuki, Akio Yoneda, Kohei Asada, Takashi Kobayashi & Hiroyoshi Naito (2007): Influence of Alkyl Chain Length on the Solid-State Packing and Fluorescence of 1,4,5,8-Tetra(alkyl)anthracenes, Molecular Crystals and Liquid Crystals, 474:1, 119-135

To link to this article: http://dx.doi.org/10.1080/15421400701617350

Mol. Cryst. Liq. Cryst., Vol. 474, pp. 119–135, 2007

ISSN: 1542-1406 print/1563-5287 online
DOI: 10.1080/15421400701617350

Influence of Alkyl Chain Length on the Solid-State Packing and Fluorescence of 1,4,5,8-Tetra(alkyl)anthracenes

Chitoshi Kitamura
Yasushi Abe
Nobuhiro Kawatsuki
Akio Yoneda
Department of Materials Science and Chemistry, Graduate School of Engineering, University of Hyogo, Himeji, Hyogo, Japan

Kohei Asada
Takashi Kobayashi
Hiroyoshi Naito
Department of Physics and Electronics, Graduate School of Engineering, Osaka Prefecture University, Sakai, Osaka, Japan

1,4,5,8-Tetra(alkyl)anthracenes (alkyl = methyl, ethyl, n-propyl, and n-hexyl) were prepared by a sequence of reactions of 1,2,4,5-tetrabromobenzene and 2,5-dialkylfurans in the presence of n-BuLi, hydrogenation, and treatment with acid. The influence of alkyl chain length on the packing patterns in the crystals and the fluorescent properties in the solid state was investigated. X-ray analysis revealed that the molecular structures can be classified into plane, semi-chair, and chair forms and that the packing patterns can be categorized into two-dimensional (herringbone) and one-dimensional (slipped-parallel) arrangements, in both of which there is no π–π stacking. In the case of the methyl, ethyl, and n-propyl derivatives, the wave shapes of the fluorescence spectra in the solid state resemble each other; on the other hand, the n-hexyl derivative displayed a slightly red-shifted and broader spectrum. The absolute quantum yield depended on the transition dipole moments because of the packing patterns and crystal rigidity. The n-propyl derivative demonstrated the highest quantum yield of $\Phi_f = 0.85$ among the tetra(alkyl)-anthracenes.

Keywords: alkyl-substituted anthracene; crystal structure; packing; quantum yield; solid-state fluorescence

Address correspondence to Chitoshi Kitamura, Department of Materials Science and Chemistry, Graduate School of Engineering, University of Hyogo, 2167 Shosha, Himeji, Hyogo 671-2280, Japan. E-mail: kitamura@eng.u-hyogo.ac.jp

INTRODUCTION

Solid-state packing effects play an important role in the performance of electronic and photonic materials [1]. Although there have been numerous reports on molecular modification by the introduction of substituents into organic fluorophores to control fluorescent properties in solution, to date, there has been relatively little research on the correlation between solid-state packing patterns and fluorescent properties [2–7]. Thus, molecular design to control solid-state fluorescence is not fully understood [4–6].

We report here the synthesis, crystal structures, and solid-state fluorescent properties of 1,4,5,8-tetra(alkyl)anthracenes **1a-d** (Fig. 1). We expected that by varying the alkyl chain length, both the molecular packing behavior and solid-state fluorescence would be varied easily. The former would depend on the balance of the intermolecular interactions between aromatic moieties, such as face-to-face (π–π stacking) and edge-to-face (CH-π) interactions, and the self-assembling ability of alkyl side chains. Anthracene was selected because it is a representative fluorescent molecule as well as belonging to the acene family, which has been receiving particular attention because of its importance as an organic semiconducting material [8]. It is well known that unsubstituted oligoacenes prefer the herringbone structure because of edge-to-face interactions between neighboring molecules in two-dimensional (2-D) layers. As shown later, a large transition dipole moment, which is one of the important factors leading to large fluorescence quantum yields, cannot be obtained in the herringbone (2-D) packing pattern of anthracene moieties. It is possible that the lateral alkyl chains act as spacers and modulate the spatial arrangement of anthracene moieties. Accordingly, the fluorescent behavior in the solid state can be adjusted by the molecular ordering of alkyl-substituted anthracene molecules. Longer alkyl chains tend to form a lamellar structure by van der Waals interactions. In the tetrathiafulvalene (TTF) series, it is well known that the longer alkyl chains serve as

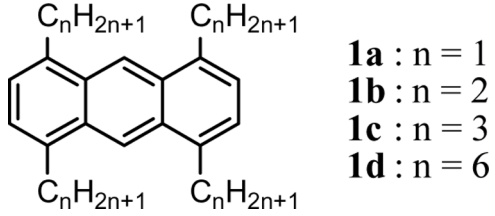

FIGURE 1 1,4,5,8-Tetra(alkyl)anthracene **1a–d**.

molecular fasteners [9], which form the molecular packing and stacking of the TTF molecules, leading to high conductivity. We thought that the intermolecular interactions between anthracene moieties can be spatially tuned by the length of alkyl chains, and as a result, the solid-state fluorescence can be chemically controlled.

EXPERIMENTAL

General

THF and toluene were distilled from $LiAlH_4$ and CaH_2, respectively, prior to use. Commercially available reagents containing 2,5-dimethylfuran (**3a**) were used as supplied unless otherwise stated. All reactions were carried out under a nitrogen atmosphere unless otherwise noted. 1,2,4,5-Tetrabromobenzene (**4**) was prepared according to the literature procedure [10]. Analytical thin-layer chromatography (TLC) was performed on Merck silica-gel 60 F_{254} 0.25 mm aluminium plates. Column chromatography was performed on Wako silica gel C-300 (45–75 μm). Melting points were determined on a Yanaco melting-point apparatus and are uncorrected. ^1H and ^{13}C NMR spectra were recorded on a Bruker-Biospin DRX500 FT spectrometer at 500 and 126 MHz, respectively. IR spectra were recorded on a Shimadzu FTIR-8400 spectrometer as KBr pressed pellets. Elemental analysis was carried out on a Yanaco MT-5 CHN corder.

General Procedure for the Synthesis of 2,5-Dialkylfurans 3

The procedure described by Cook *et al*. [11] was modified. To an ice-cooled mixture of furan **2** (2.0 mL, 27.6 mmol) and TMEDA (9.4 mL, 62.3 mmol), a solution of *n*-BuLi in *n*-hexane (40 mL, 1.54 M, 61.6 mmol) was added slowly, and then the mixture was refluxed for 1 h. During the heating time, the mixture changed to a brown suspension. The solution was allowed to be cooled to rt and cooled with an ice bath. A solution of 1-bromoalkane (82.9 mmol) in THF (20 mL) was added dropwise to the suspension. The mixture was stirred at rt for 21.5 h. After quenching with water, the crude product was extracted with Et_2O, washed with brine, and dried over Na_2SO_4. After evaporation of the solvent, the residue was subjected to silica-gel chromatography ($CHCl_3$/*n*-hexane = 1:1) and dried under vacuum with a mild heating to remove unreacted 1-bromoalkane and monosubstituted furan. The product obtained was used without further purification in the next reaction except that the purification of **3b** was carried out by distillation (bp 138°C, lit. [11] 138°C).

2,5-Diethylfuran (3b)

Yield, 51%. ^{1}H NMR (500 MHz, $CDCl_3$) δ 1.21 (t, $J = 7.4$ Hz, 6H, $2CH_3$), 2.60 (t, $J = 7.4$ Hz, 4H, $2CH_2$), 5.85 (s, 2H, 3,4-H).

2,5-Di(n-propyl)furan (3c)

Yield, 40%. ^{1}H NMR (500 MHz, $CDCl_3$) δ 0.95 (t, $J = 7.4$ Hz, 6H, $2CH_3$), 1.60–1.67 (m, 4H, $2CH_2$), 2.54 (t, $J = 7.4$ Hz, 4H, $2CH_2$), 5.85 (s, 2H, 3,4-H).

2,5-Di(n-hexyl)furan (3d)

Yield, 66%. ^{1}H NMR (500 MHz, $CDCl_3$) δ 0.88 (t, $J = 6.8$ Hz, 6H, $2CH_3$), 1.26–1.37 (m, 4H, $2CH_2$), 1.55–1.63 (m, 12H, $6CH_2$), 2.56 (t, $J = 7.6$ Hz, 4H, $2CH_2$), 5.83 (s, 2H, 3,4-H).

General Procedure for the Synthesis of *syn/anti*

1,4:5,8-Diepoxy-1,4:5,8-tetra(alkyl)anthracenes 5

A mixture of **3** (13.3 mmol) and **4** (2.10 g, 5.34 mmol) in toluene (45 mL) was cooled to -30°C. To the mixture, a solution of *n*-BuLi in *n*-hexane (10 mL, 1.58 M, 15.8 mmol) was added dropwise over 1 h. Then the mixture was warmed up to rt over 2 h and stirred at rt for additional 5 h. After quenching with water, the aqueous layer was extracted with $CHCl_3$. The combined organic layer was washed with brine and dried over Na_2SO_4. After evaporation, the residue was subjected to silica-gel chromatography ($CHCl_3$/*n*-hexane = 1:1 → $CHCl_3$ → $CHCl_3$/AcOEt = 10:1) to afford *syn*/*anti* bis(furan)adducts **5** as a mixture of a viscous orange oil and a white solid (in the case of **5d**, only a brown oil). In the case of *syn*/*anti* **5c**, washing the adducts with *n*-hexane provided pure *anti* **5c**, which was confirmed by X-ray analysis and was characterized by ^{1}H NMR [12]. ^{1}H NMR of **5** showed that the *syn*/*anti* ratios were *ca.* 1:1.

syn/anti 1,4:5,8-Diepoxy-1,4:5,8-tetramethylanthracene (5a)

Yield, 70%. ^{1}H NMR (500 MHz, $CDCl_3$) δ 1.86 (s, 12H, $4CH_3$, *anti*), 1.87 (s, 12H, $4CH_3$, *syn*), 6.77 (s, 4H, 2,3,6,7-H, *syn*), 6.78 (s, 4H, 2,3,6,7-H, *anti*), 6.96 (s, 2H, 9,10-H, *anti*), 6.97 (s, 2H, 9,10-H, *syn*).

syn/anti 1,4:5,8-Diepoxy-1,4:5,8-tetraethylanthracene (5b)

Yield, 49%. ^{1}H NMR (500 MHz, $CDCl_3$) δ 1.15 (t, $J = 7.5$ Hz, 24H, $8CH_3$, *syn* and *anti*), 2.21–2.34 (m, 16H, $8CH_2$, *syn* and *anti*), 6.78 (s, 4H, 2,3,6,7-H, *anti*), 6.79 (s, 4H, 2,3,6,7-H, *syn*), 6.92 (s, 2H, 9,10-H, *syn*), 6.93 (s, 2H, 9,10-H, *syn*).

syn/anti 1,4:5,8-Diepoxy-1,4:5,8-tetra(n-propyl)anthracene (5c)

Yield, 66%. ^{1}H NMR (500 MHz, $CDCl_3$) δ 1.04 (t, $J = 7.4$ Hz, 24H, $8CH_3$, *syn* and *anti*), 1.55–1.65 (m, 16H, $8CH_2$, *syn* and *anti*),

2.10–2.28 (m, 16H, 8CH_2, *syn* and *anti*), 6.75 (s, 4H, 2,3,6,7-H, *anti*), 6.76 (s, 4H, 2,3,6,7-H, *syn*), 6.89 (s, 4H, 9,10-H, *syn* and *anti*).

syn/anti 1,4:5,8-Diepoxy-1,4:5,8-tetra(n-hexyl)anthracene (5d)

Yield, 42%. ^{1}H NMR (500 MHz, $CDCl_3$) δ 0.90 (t, $J = 6.8$ Hz, 24H, 8CH_3, *syn* and *anti*), 1.32–1.63 (m, 64H, 32CH_2, *syn* and *anti*), 2.15–2.26 (m, 16H, 8CH_2, *syn* and *anti*), 6.74 (s, 4H, 2,3,6,7-H, *anti*), 6.76 (s, 4H, 2,3,6,7-H, *syn*), 6.89 (s, 4H, 9,10-H, *syn* and *anti*).

General Procedure for the Synthesis of 1,4,5,8-Tetra(alkyl)anthracene 1

syn/*anti* **5** (0.48 mmol) in EtOH (20 mL) and *n*-BuOH (1 mL) were hydrogenated over 10% Pd/C (30 mg) under atmospheric pressure at rt for 3 h. The catalyst was removed by filtration, and the filtrate was evaporated under reduced pressure. To the residue, an ice-cooled solution of conc. HCl (4 mL) and Ac_2O (20 mL) was added. The mixture was stirred at rt for 3 h. After cooling with ice, water was added into the mixture. The resultant mixture was extracted with $CHCl_3$, and the extract was washed with aqueous Na_2CO_3 and brine and dried over Na_2SO_4. After evaporation of the solvent, column chromatography on silica gel with ($CHCl_3$/*n*-hexane = 1:1) gave the corresponding 1,4,5,8-tetra(alkyl)anthracene **1**.

1,4,5,8-Tetramethylanthracene (1a)

Compound **1a** was obtained in 73% yield from **5a** as a pale yellow solid (from *n*-hexane), mp 219–221°C; lit. [13] 219°C. ^{1}H NMR (500 MHz, $CDCl_3$) δ 2.81 (s, 12H, 4CH_3), 7.22 (s, 4H, 2,3,6,7-H), 8.64 (s, 2H, 9,10-H).

1,4,5,8-Tetraethylanthracene (1b)

Compound **1b** was obtained in 18% yield from **5b** as a pale yellow solid (from *n*-hexane), mp 120–121°C. The yield was the lowest because some unidentified products were formed. ^{1}H NMR (500 MHz, $CDCl_3$) δ 1.48 (t, $J = 7.4$ Hz, 12H, 4CH_3), 3.25 (q, $J = 7.4$ Hz, 8H, 4CH_2), 7.26 (s, 4H, 2,3,6,7-H), 8.83 (s, 2H, 9,10-H). ^{13}C NMR (126 MHz, $CDCl_3$) δ 14.81, 26.11, 119.59, 123.63, 129.98, 138.28. FTIR (KBr) 2960.5, 2935.5, 2873.7, 1618.2, 1460.0, 1296.1, 842.8 cm^{-1}. Anal. calcd. for $C_{22}H_{26}$: C, 90.98; H, 9.02%. Found: C, 90.73; H, 9.20%.

1,4,5,8-Tetra(n-propyl)anthracene (1c)

Compound **1c** was obtained in 74% yield from **5c** as a pale yellow solid (from *n*-hexane), mp 106–108°C. ^{1}H NMR (500 MHz, $CDCl_3$)

δ 1.08 (t, $J = 7.3$ Hz, 12H, $4CH_3$), 1.85–1.92 (m, 8H, $4CH_2$), 3.16 (t, $J = 7.7$ Hz, 8H, $4CH_2$), 7.22 (s, 4H, 2,3,6,7-H), 8.79 (s, 2H, 9,10-H). ^{13}C NMR (126 MHz, $CDCl_3$) δ 14.44, 23.80, 35.61, 119.96, 124.68, 130.06, 136.77. FTIR (KBr) 2956.7, 2929.7, 2869.9, 1629.7, 1465.8, 873.7, 835.1 cm^{-1}. Anal. calcd. for $C_{26}H_{34}$: C, 90.11; H, 9.89%. Found: C, 90.10; H, 10.04%.

1,4,5,8-Tetra(n-hexyl)anthracene (1d)

Compound **1d** was obtained in 72% yield from **5d** as a pale yellow solid (from *n*-hexane), mp 94–96°C. ^{1}H NMR (500 MHz, $CDCl_3$) δ 0.90 (t, $J = 6.9$ Hz, 12H, $4CH_3$), 1.31–1.40 (m, 8H, $4CH_2$), 1.48–1.53 (m, 16H, $8CH_2$), 1.81–1.87 (m, 8H, $4CH_2$), 3.17 (t, $J = 7.6$ Hz, 8H, $4CH_2$), 7.22 (s, 4H, 2,3,6,7-H), 8.80 (s, 2H, 9,10-H). ^{13}C NMR (126 MHz, $CDCl_3$) δ 14.16, 22.79, 29.84, 30.93, 31.93, 33.70, 120.02, 124.62, 130.07, 137.06. FTIR (KBr) 2956.7, 2925.8, 2850.6, 1467.7, 873.7 cm^{-1}. Anal. calcd. for $C_{38}H_{58}$: C, 88.65; H, 11.35%. Found: C, 88.93; H, 11.40%.

Crystal Structure Determinations

Crystals of compounds **1a–d** were grown from *n*-hexane. The single-crystal data were collected on a Rigaku/Mercury CCD diffractometer with Mo-Kα radiation ($\lambda = 0.71070$ Å). The structure was solved by a direct method using SIR92 [14] and refined by the full matrix least-squares method on F^2 with anisotropic temperature factors for non-hydrogen atoms. Hydrogen atoms were refined isotropically. All of the calculations were performed using the teXsan program packages [15]. Full crystallographic details, excluding structure factors, for the structures of compounds **1a** (CCDC 296864), **1b** (CCDC 296865), **1c** (CCDC 296866), and **1d** (CCDC 296867) have been deposited with the Cambridge Crystallographic Data Centre. Copies of the data can be obtained, free of charge, via http://www.ccdc.cam.ac.uk/conts/retrieving.html (or form the Cambridge Crystallographic Data Centre, 12 Union Road, Cambridge, CB2 1EZ, UK; Fax: +44 1223 336033; e-mail: deposit@ccdc.ca.ac.uk).

Crystal Data for 1a

$C_{18}H_{18}$, $M = 234.34$, monoclinic, $P2_1/c$, $a = 9.880(2)$, $b = 5.0470(5)$, $c = 13.239(2)$ Å, $\beta = 101.501(7)^\circ$, $V = 646.9(2)$ Å^3, $Z = 2$, $T = 223$ K, $D_c = 1.203$ g cm^{-3}, μ (MoKa) = 0.67 cm^{-1}, 5172 reflections measured, 4936 unique ($R_{int} = 0.025$), GoF = 0.89, 118 parameters refined, final R-factors $R_1 = 0.053$ for 1164 reflections with $I > 2\sigma(I)$, $wR_2 = 0.213$ for all data.

Crystal Data for 1b

$C_{22}H_{26}$, $M = 290.45$, monoclinic, $P2_1/n$, $a = 10.208(1)$, $b = 5.1793(5)$, $c = 15.681(2)$ Å, $\beta = 92.587(7)^\circ$, $V = 828.2(2)$ Å^3, $Z = 2$, $T = 223$ K, $D_c = 1.165$ g cm^{-3}, μ (MoKa) $= 0.65$ cm^{-1}, 6381 reflections measured, 1835 unique ($R_{int} = 0.023$), GoF $= 1.58$, 152 parameters refined, final R-factors $R_1 = 0.052$ for 1627 reflections with $I > 2\sigma(I)$, $wR_2 = 0.155$ for all data.

Crystal Data for 1c

$C_{26}H_{34}$, $M = 346.55$, triclinic, $P\ \bar{1}$, $a = 6.5551(1)$, $b = 7.9150(2)$, $c = 10.9768(1)$ Å, $\alpha = 108.01(1)$, $\beta = 72.29(1)$, $\gamma = 102.05(2)^\circ$, $V = 511.80(5)$ Å^3, $Z = 1$, $T = 223$ K, $D_c = 1.124$ g cm^{-3}, μ (MoKa) $= 0.62$ cm^{-1}, 3792 reflections measured, 2205 unique ($R_{int} = 0.051$), GoF $= 1.61$, 118 parameters refined, final R-factors $R_1 = 0.063$ for 2043 reflections with $I > 2\sigma(I)$, $wR_2 = 0.217$ for all data.

Crystal Data for 1d

$C_{38}H_{58}$, $M = 514.88$, triclinic, $P\ \bar{1}$, $a = 4.731(4)$, $b = 12.81(1)$, $c = 14.13(1)$ Å, $\alpha = 78.45(2)$, $\beta = 77.32(2)$, $\gamma = 84.94(3)^\circ$, $V = 817(1)$ Å^3, $Z = 1$, $T = 173$ K, $D_c = 1.046$ g cm^{-3}, μ (MoKa) $= 0.58$ cm^{-1}, 6439 reflections measured, 3638 unique ($R_{int} = 0.048$), GoF $= 1.30$, 288 parameters refined, final R-factors $R_1 = 0.095$ for 2310 reflections with $I > 2\sigma(I)$, $wR_2 = 0.186$ for all data.

Fluorescence Measurements in the Solid State

The crystals were excited by He-Cd laser (Kimmon, IK3301R-G), and the spectra were recorded using a calibrated optical multichannel analyzer (Hamamatsu Photonics, PMA11). The measurement of the absolute quantum yield was performed using an integrating sphere (Labsphere, IS-040-SF).

RESULTS AND DISCUSSION

Synthesis and Optical Properties in Solution

The synthesis of 1,4,5,8-tetramethylanthracene from 2,5-dimethylfuran and transient bis(aryne) using the Diels–Alder reaction has been reported [12]. We improved the method to obtain alkyl-substituted anthracenes simply (Scheme 1). First, we prepared 2,5-dialkylfurans **3** by direct dilithiation of furan **2** in the presence of *N*,*N*,*N*′,*N*′-tetramethylethylenediamine (TMEDA) in 40–66% yield, although

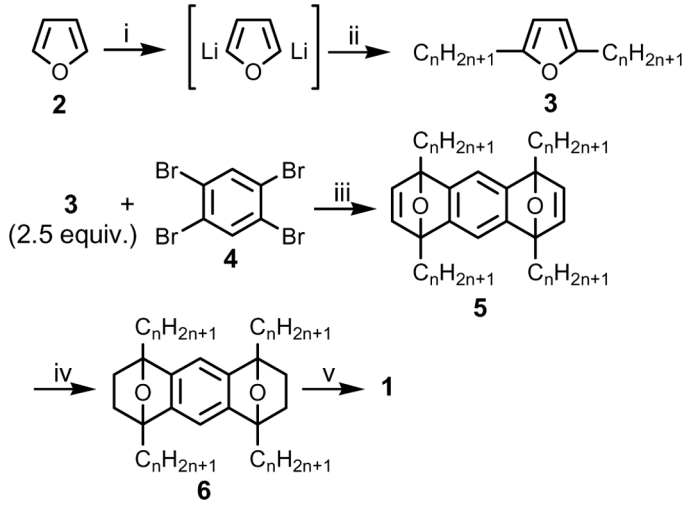

SCHEME 1 Reagents and conditions: i, *n*-BuLi (2.2 equiv.), TMEDA (2.2 equiv.), *n*-hexane, reflux; ii, 1-bromoalkane (3 equiv.), THF, rt, 40–66% (two-steps, from **2**); iii, *n*-BuLi (3 equiv.), toluene, -30°C to rt, 42–70%; iv, H_2, 10% Pd/C, 20:1 EtOH–*n*-BuOH; v, conc. HCl, Ac_2O, 18–74% (two-steps, from **5**).

3 could be obtained by a two-step lithiation/alkylation procedure that was time-consuming [11]. Next, 1,2,4,5-tetrabromobenzene (**4**) in the presence of 2.5 equiv. of **3** was treated with 3 equiv. of *n*-BuLi to give the corresponding anthracene intermediate **5** in 42–70% yield as a mixture of *syn* and *anti* stereoisomers. The *syn*/*anti* ratios in **5** were *ca*. 1:1 as revealed by ^{1}H NMR. In the case of **5c**, the *anti* isomer could be isolated as a white solid purely by filtration and washing with *n*-hexane and was characterized by X-ray crystallography [16]. On the basis of the ^{1}H NMR spectrum of isolated *anti*-**5c**, the assignment of signals of the *syn* isomer in a *syn*/*anti* mixture became possible. Thus, understanding the chemical shifts of *syn* and *anti* isomers led to the differentiation between *syn* and *anti* isomers in ^{1}H NMR. Transformation of **5** into anthracene **1** was achieved by a facile sequence of catalytic hydrogenation in alcohols and then dehydration of **6** with acid in 18–74% yield. The solubility of compounds **1a–d** in organic solvents was investigated, and they showed good solubility in hydrocarbon solvents such as *n*-hexane.

The absorption and fluorescence spectra of **1a–d** in *n*-hexane are shown in Fig. 2, and the spectral data are summarized in Table 1.

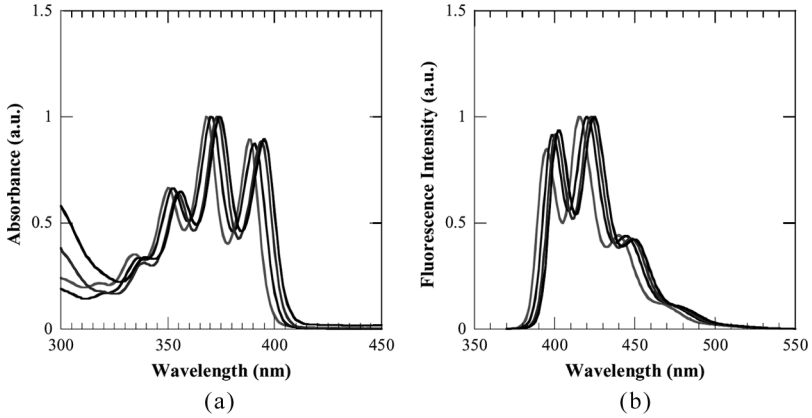

FIGURE 2 (a) Absorption and (b) fluorescence spectra in *n*-hexane of **1a** (red), **1b** (blue), **1c** (green), and **1d** (black). Concentration: **1a**, 5.53×10^{-5} M; **1b**, 4.48×10^{-5} M; **1c**, 3.79×10^{-5} M; **1d**, 4.55×10^{-5} M.

As we expected, there is no marked differences in the wave shape, the wavelengths of the absorption and fluorescence peaks, and the fluorescence quantum yield (Φ_f values are around 0.3) among **1a–d** because the molecules exist in an almost monodispersed state in a dilute solution. Both the absorption and fluorescence spectra showed the vibrational structure, in which the band assigned as the 0–1 transition was the highest, and their peaks shifted slightly to longer wavelengths with increasing alkyl chain length.

TABLE 1 UV–Vis Absorption and Fluorescence Properties of **1a–d** in *n*-Hexane

Compound	Absorption spectral data[a], λ_{max} (log ε) (nm)	Fluorescence spectral data[a]	
		λ_{em}[b] (nm)	Φ_f[c]
1a	350 (3.71), 368 (3.88), 388 (3.83)	395, 415, 440	0.32
1b	352 (3.74), 369 (3.92), 391 (3.87)	399, 420, 444	0.25
1c	355 (3.78), 373 (3.97), 394 (3.92)	401, 423, 448	0.31
1d	356 (3.71), 374 (3.90), 395 (3.85)	402, 425, 450	0.36

[a]Peaks based on the 0–0, 0–1, and 0–2 transitions.
[b]Excited at 355 nm.
[c]Fluorescence quantum yields were determined using 9,10-diphenylanthracene as the standard.

X-ray Crystal Structures

To investigate the effect of changing the length of the alkyl chain on the packing pattern in the crystal, we carried out X-ray crystallographic analysis of **1a–d**. With an increase in the alkyl chain length, the interactions between alkyl chains were expected to induce stronger molecular ordering. All single crystals were obtained by slow evaporation from their *n*-hexane solutions. The crystal systems were the monoclinic space group $P2_1/c$ with $Z = 2$ for **1a**, monoclinic space group $P2_1/n$ with $Z = 2$ for **1b**, triclinic space group $P\bar{1}$ with $Z = 1$ for **1c**, and triclinic space group $P\bar{1}$ with $Z = 1$ for **1d**. The molecular packing patterns in the crystals are depicted in Fig. 3. All of the molecules of **1a–d** possess a center of symmetry, and halves of the formula units are crystallographically independent because of the high symmetry of the molecules. The anthracene units are strictly planar. Interestingly, longer alkyl side chains than ethyl groups produced a

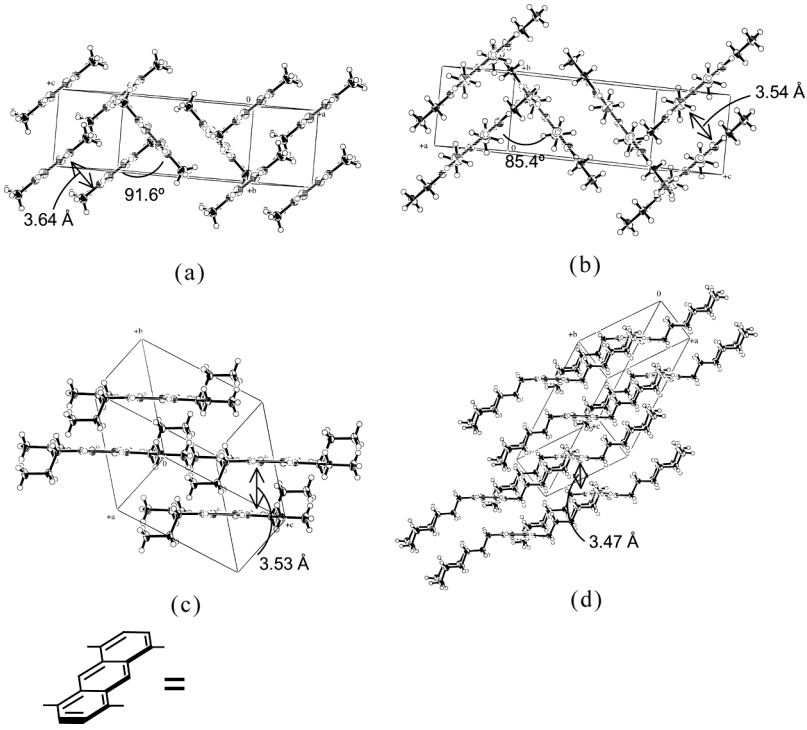

FIGURE 3 Packing diagrams for (a) **1a**, (b) **1b**, (c) **1c**, and (d) **1d**.

striking change in the packing patterns. When viewed down the long molecular axis, both **1a** and **1b** appear to be stacked in the herringbone structure (Figs. 3a and 3b) in a similar manner to nonsubstituted anthracene [17], indicating 2-D arrangements. In addition, the packing patterns do not adopt π–π stacking (face-to-face overlap of anthracene moieties). The interplanar tilt angles between anthracene rings in two adjacent columns are 91.6° for **1a** and 85.4° for **1b**, respectively. On the other hand, the anthracene rings in both **1c** and **1d** adopt a slipped-parallel pattern without π–π stacking along the anthracene column direction (Figs. 3c and 3d), exhibiting one-dimensional (1-D) arrangements. Further, the anthracene units in **1c** and **1d** form an anthracene plane.

In the crystals of **1a** and **1b**, the alkyl side chains are essentially planar with the anthracene ring, as shown in Fig. 4a. In the crystal of **1c**, a pair of two *n*-propyl groups at the 1 and 5 positions take a coplanar conformation with the anthracene ring, while another pair of two *n*-propyl groups at the 4 and 8 positions extend upward and downward toward the out-of-plane anthracene directions (Fig. 4b). In addition, **1d** in the crystal is a stair-like molecule in which two *n*-hexyl groups at the 1 and 8 positions extend upward and another two *n*-hexyl groups at the 4 and 5 positions extend downward out of the anthracene plane (Fig. 4c). The alkyl chains of **1c** and **1d** take an all-*trans* conformation like other hydrocarbon chains frequently found in X-ray analysis. We refer to the molecular structures of **1b**, **1c**, and **1d** as plane, semi-chair, and chair forms, respectively. The formation of three different conformations results from the torsion degrees of freedom in the alkyl chain.

Figure 5 shows the stacking patterns of two vicinal molecules. Regarding the solid-state fluorescence, the translational shift of neighboring molecules in the stack is an essential factor to understanding the fluorescence behavior. In **1a–d**, distinct stacking patterns are observed. Undoubtedly, there is no spatial overlap of anthracene moieties on adjacent molecules. The slip distances between neighboring molecules are 5.05, 5.18, 6.56, and 4.74 Å for **1a**, **1b**, **1c**, and **1d**, respectively. Compound **1c** has the longest slip distance, and **1d** has the shortest distance. As shown in Fig. 3, the interplanar distances between anthracene moieties are 3.64, 3.54, 3.53, and 3.47 Å for **1a**, **1b**, **1c**, and **1d**, respectively. The shortest distance for overlapping nonbonded atoms in anthracene for **1a** is 3.67–3.68 Å, which is longer compared with other anthracenes (3.58 Å for **1b**, 3.59 Å for **1c**, and 3.56–3.59 Å for **1d**). As a result, the displacements between neighboring anthracene moieties are the largest in **1c** and the smallest in **1d**. It can be recognized that the hexyl groups in **1d** greatly affect the dense

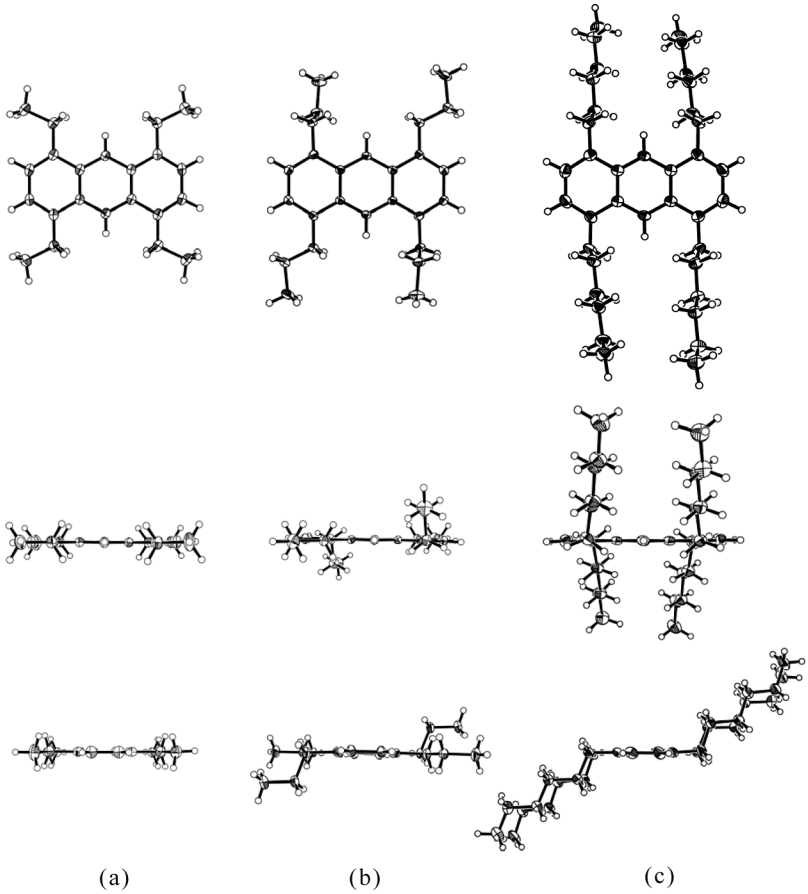

FIGURE 4 Molecular structures of (a) **1b**, (b) **1c**, and (c) **1d**. Upper, middle, and lower structures show top view, side view, and view along the long molecular axis, respectively.

packing arrangement, suggesting that molecular fasteners are effective in crystallization.

In a series of these observations, the length of the alkyl side chains strongly affects not only the molecular geometry but also the crystal packing arrangement. The interactions related to the specific arrangements can be roughly classified into two types: (1) interactions between aromatic units and (2) interactions between alkyl chains. The former may be more favorable than the latter in **1a** and **1b** where the herringbone structure, frequently found in oligoacenes [8], can be

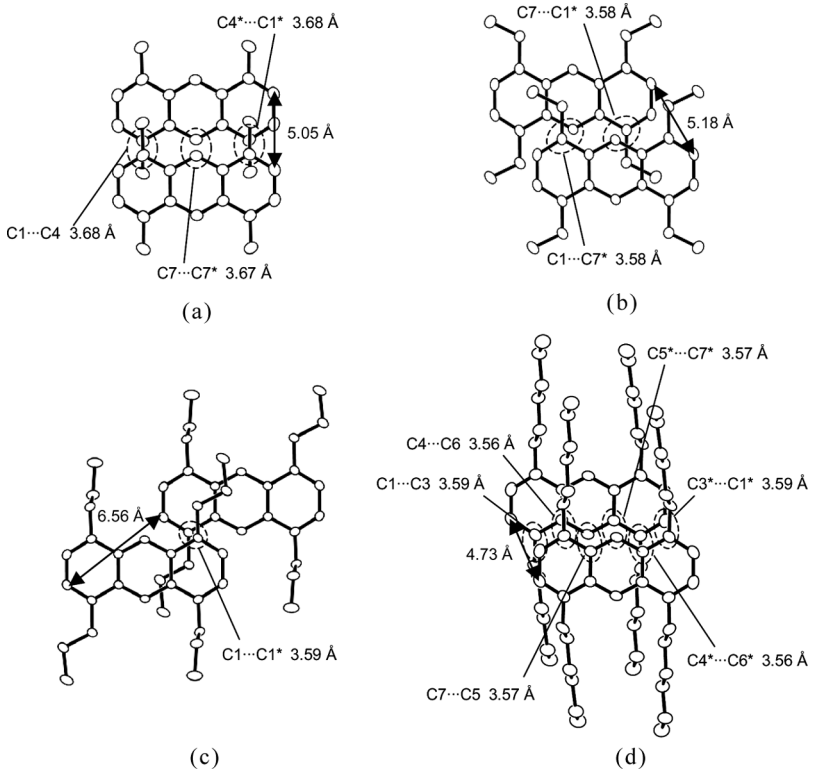

FIGURE 5 Stacking patterns of two vicinal molecules of (a) **1a**, (b) **1b**, (c), **1d**, and (d) **1d**. Hydrogen atoms are omitted for clarity.

seen. On the other hand, the elongation of alkyl chains over 2 carbon atoms seems to enhance the latter. In **1c** and **1d**, the molecules are arranged in stacks showing a parallel orientation of the anthracene moiety, and two columnar structures consisting of aromatic and alkyl regions can be observed. In particular, the hexyl groups in **1d** promote the lamellar structure and lead to the dense packing of anthracene moieties.

Fluorescence in the Solid State

To examine the influence of crystal packing on the solid-state fluorescence properties, the fluorescence spectra of crystals of **1a–d** and the absolute quantum yields were measured. The fluorescence spectra of crystals of **1a–d** are shown in Fig. 6, and their spectral data are

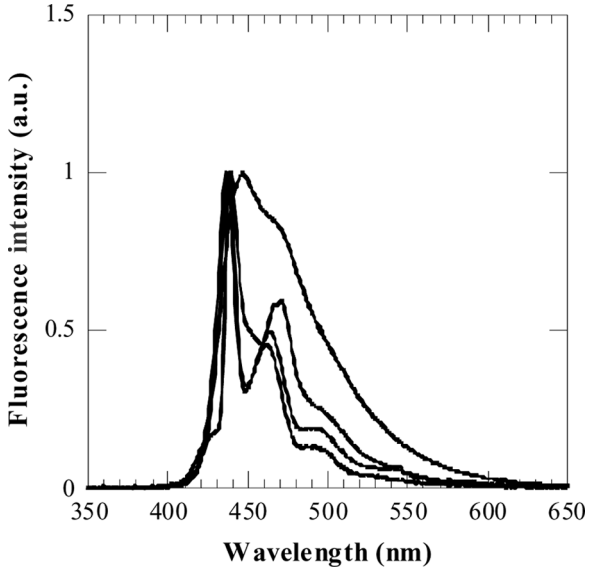

FIGURE 6 Fluorescence spectra of **1a** (red), **1b** (blue), **1c** (green), and **1d** (black) in the solid state, excited at 325 nm.

summarized in Table 2. The fluorescence properties in the solid state are dependent on packing pattern. All of the fluorescence spectra in the solid state are red-shifted with respect to those in solution, indicating the presence of intermolecular interactions in the crystals. The crystals of **1a–c** illustrate similar sharp fluorescence spectra, which can be attributed to free exciton luminescence. Fluorescence maxima were observed at 436–439 nm. On the other hand, the crystal of **1d** illustrates a slightly red-shifted and broader fluorescence spectrum with a fluorescence maximum at 447 nm and a shoulder peak around

TABLE 2 Structural and Fluorescence Properties of **1a–d** in the Solid State

	Structural data		Fluorescence spectral data	
Compound	Molecular structure	Packing mode	$\lambda_{em}{}^{a}$/nm	$\Phi_f{}^{b}$
1a	Plane form	herringbone	438, 462	0.39
1b	Plane form	herringbone	439, 471	0.68
1c	Semi-chair form	slipped-parallel	436, 462	0.85
1d	Chair form	slipped-parallel	447	0.36

[a]Excited at 325 nm.
[b]Absolute quantum yield in the solid state.

480 nm. It is well known that in pyrene crystal, the pyrene excimer forms a more stable excited state compared with the free exciton state because of large lattice-relaxation energy, and red-shifted and broad fluorescence derived from the excimer is dominant [18]. Another feature of excimer emission is its low quantum yield, which results from enhancement of nonradiative decay of excited states because of lattice relaxation to form the excimer. In the crystal of **1d**, the molecular packing is not expected to be rigid because of an abundance of flexible long alkyl groups; the slip distance between two adjacent anthracenes in one column (4.73 Å) is the shortest among **1a–d** (slip distances: **1a**, 5.05 Å; **1b**, 5.18 Å; **1c**, 6.56 Å), probably resulting in anthracene excimer formation and relatively low quantum yield ($\Phi_f = 0.36$). On the other hand, the quantum yields of crystals of **1a** ($\Phi_f = 0.39$), **1b** ($\Phi_f = 0.68$), and **1c** ($\Phi_f = 0.85$) can be understood in terms of their packing patterns. According to free exciton theory, all of the molecules within the coherent size of a free exciton contribute to enhance the macroscopic transition dipole moment between the lowest excited state and the ground state. However, when the crystal adopts a 2-D arrangement as well as has two molecules in the unit cell, the excited state of the molecule in the crystal splits into two energy levels (Davydov splitting), and then the transition dipole moment from the lower split level to the ground state (this transition dipole moment is an essential factor in the fluorescence quantum yield) can be zero, depending on the packing patterns [19]. In such a case, the magnitude of the solid-state fluorescence can be roughly estimated from linear combination of the transition dipole moments of the two molecules that have different orientations in the unit cell. Because, in the crystal of **1a**, the transition dipole moments of the two anthracenes (two distinguishable directions along the short molecular axes of anthracene moieties in two adjacent columns) are perpendicular (90.0°) to each other, only 50% of the possible transition dipole moment is distributed to the transition from the lower split state in the crystal. In the crystal of **1b**, the angle between directions along the short molecular axes of the two anthracene moieties in the unit cell (117.2°) is larger than 90°, and consequently more than 50% of the possible transition dipole moment contributes to the transition from the lower split state to the ground state. In contrast to the crystals of **1a** and **1b**, the crystal of **1c** has a parallel 1-D arrangement and has one molecule in the unit cell, and so all possible transition dipole moments concentrate on the transition from the lowest excited state to the ground state. Therefore, under assumptions that the crystals of **1a–c** have similar nonradiative decay rates and that the decrease in crystal rigidity is not serious within the side-chain length of the *n*-propyl group, a higher quantum

yield is expected as the transition dipole moment increases, *i.e.*, **1c** > **1b** > **1a**. In some organic materials, π–π stacking results in suppression of the fluorescence quantum yield [5a,20]. In these materials, the transition dipole moments of the molecules in the unit cell are almost parallel to each other, and such molecular arrangements do not distribute any transition dipole moments to the transition between the lowest excited state and the ground state. Thus, the crystal of **1c** demonstrates that the conditions of a 1-D packing pattern, especially the same direction of transition dipole moments and not too-soft crystal rigidity, would play a significant role in the high fluorescence quantum yield in the solid state.

CONCLUSIONS

1,4,5,8-Tetra(alkyl)anthracenes (**1a–d**) were prepared from the Diels–Alder reaction of bis(aryne) and 2,5-dialkylfurans. The structural features in the crystals were characterized by X-ray analysis. The change in alkyl side chain length of anthracene led to a drastic difference in molecular and crystal structures. In the packing patterns, the methyl and ethyl derivatives (**1a** and **1b**) have 2-D arrangements; on the other hand, the *n*-propyl and *n*-hexyl derivatives (**1c** and **1d**) adopt 1-D arrangements. The packing mode affected the fluorescence properties in the solid state. The fluorescence spectra of **1a–c** exhibited similarity in shape and wavelength, whereas **1d** was slightly red-shifted and had a broader spectrum. Among **1a–d**, the crystal of **1c** exhibited the most intense fluorescence in the solid state. The fluorescence quantum yields in the solid state correlate with the transition dipole moments derived from arrangements of the anthracene ring in the unit cell as well as the crystal rigidity.

ACKNOWLEDGMENTS

We thank the Instrument Center, the Institute for Molecular Science, for assistance in obtaining X-ray data. This work was supported by a grant-in-aid (No. 18750123) from the Ministry of Education, Culture, Sports, Science, and Technology, Japan. The Hyogo Science and Technology Association is gratefully acknowledged for financial support.

REFERENCES

[1] Curtis, M. D., Cao, J., & Kampf, J. W. (2004). *J. Am. Chem. Soc.*, *126*, 4318.
[2] Langhals, H., Potrawa, T., Nöth, H., & Linti, G. (1989). *Angew. Chem., Int. Ed.*, *28*, 478.

[3] Cotrait, M., Marsau, P., Kessab, L., Grelier, S., Nourmanode, A., & Castellan, A. (1994). *Aust. J. Chem.*, *47*, 423.
[4] (a) Yoshida, K., Ooyama, Y., Miyazaki, H., & Watanabe, S. (2002). *J. Chem. Soc., Perkin Trans.*, *2*, 700; (b) Yoshida, K., Ooyama, Y., Tanikawa, S., & Watanabe, S. (2002). *J. Chem. Soc., Perkin Trans.*, *2*, 708; (c) Ooyama, Y., Nakamura, T., & Yoshida, K. (2005). *New J. Chem.*, *29*, 439; (d) Ooyama, Y. & Yoshida, K. (2005). *New J. Chem.*, *29*, 1204.
[5] (a) Mizobe, Y., Tohnai, N., Miyata, M., & Hasegawa, Y. (2005). *Chem. Commun.*, 1839; (b) Mizobe, Y., Ito, H., Hisaki, I., Miyata, M., Hasegawa, Y., & Tohnai, N. (2006). *Chem. Commun.*, 2126; (c) Mizobe, Y., Miyata, M., Hisaki, I., Hasegawa, Y., & Tohnai, N. (2006). *Org. Lett.*, *8*, 4295.
[6] (a) Matsumoto, S., Tokunaga, W., Miura, H., & Mizuguchi, J. (2001). *Bull. Chem. Soc. Jpn.*, *74*, 471; (b) Horiguchi, E., Matsumoto, S., Funabiki, K., & Matsui, M. (2005). *Bull. Chem. Soc. Jpn.*, *78*, 1167; (c) Matsumoto, S., Uchida, Y., & Yanagita, M. (2006). *Chem. Lett.*, *35*, 654; (d) Horiguchi, E., Matsumoto, S., Funabiki, K., & Matsui, M. (2006). *Bull. Chem. Soc. Jpn.*, *79*, 799.
[7] Dreuw, A., Plötner, J., Lorenz, L., Wachtveitl, J., Djanhan, J. E., Brüning, J., Metz, T., Bolte, M., & Schmidt, M. U. (2005). *Angew. Chem., Int. Ed.*, *44*, 7783.
[8] Bendikov, M., Wudl, F., & Perepichka, D. F. (2004). *Chem. Rev.*, *104*, 4891.
[9] (a) Inokuchi, H., Saito, G., Wu, P., Seki, K., Tang, T. B., Mori, T., Imaeda, K., & Yasuoka, N. (1986). *Chem. Lett.*, *15*, 1263; (b) Imaeda, K., Enoki, T., Shi, Z., Wu, P., Okada, N., Yamochi, H., Saito, G., & Inokuchi, H. (1987). *Bull. Chem. Soc. Jpn.*, *60*, 3163.
[10] Hart, H., Bashir-Hashemi, A., Luo, J., & Meador, M. A. (1986). *Tetrahedron*, *42*, 1641.
[11] McKeown, N. B., Chambrier, I., & Cook, M. J. (1990). *J. Chem. Soc., Perkin Trans.*, *1*, 1169.
[12] Hart, H., Lai, C., Nwokogu, G., Shamouilian, S., Teuerstein, A., & Zlotogorski, C. (1980). *J. Am. Chem. Soc.*, *102*, 6651.
[13] Hart, H., Raju, N., Meador, M. A., & Ward, D. L. (1981). *J. Org. Chem.*, *46*, 1251.
[14] Altmare, A., Burla, M. C., Camalli, M., Cascarano, M., Giacovazzo, C., Guagliardi, A., & Polidori, G. (1994). *J. Appl. Cryst.*, *27*, 435.
[15] Crystal Structure Analysis Package, Molecular Structure Corporation (1985, 1999). The Woodlands, Texas.
[16] Kitamura, C., Abe, Y., Ouchi, M., & Yoneda, A. (2004). *Anal. Sci.*, *20*, x27.
[17] Brock, C. P. & Dunitz, J. D. (1990). *Acta Cryst.*, *B46*, 795.
[18] Song, K. S. & Williams, R. T. (1993). *Self-Trapped Excitons*, Springer-Verlag: Berlin, Chap. 8, p. 300.
[19] Davydov, A. S. (1971). *Theory of Molecular Excitons*, Plenum Press: New York.
[20] Spano, F. C. (2005). *J. Chem. Phys.*, *122*, 234701.